

# The European Large Area *ISO* Survey — II. Mid-infrared extragalactic source counts

## Journal Item

Mon. Not. R. Astron. Soc. **316**, 768–778 (2000)

# The European Large Area *ISO* Survey – II. Mid-infrared extragalactic source counts

Stephen Serjeant,[1★] Seb Oliver,[1†] Michael Rowan-Robinson,[1] Hans Crockett,[1] Vasilis Missoulis,[1] Tim Sumner,[1] Carlotta Gruppioni,[1,2] Robert G. Mann,[1,7] Nick Eaton,[1] David Elbaz,[3] David L. Clements,[11,4] Amanda Baker,[3,4] Andreas Efstathiou,[1] Catherine Cesarsky,[3] Luigi Danese,[13] Alberto Franceschini,[5] Reinhardt Genzel,[6] Andy Lawrence,[7] Dietrich Lemke,[8] Richard G. McMahon,[9] George Miley,[10] Jean-Loup Puget[11] and Brigitte Rocca-Volmerange[12]

[1]*Astrophysics Group, Blackett Laboratory, Imperial College of Science Technology & Medicine, Prince Consort Rd, London SW7 2BZ*
[2]*Osservatorio Astronomico di Bologna, via Ranzani 1, 40127 Bologna, Italy*
[3]*CEA / SACLAY, 91191 Gif sur Yvette cedex, France*
[4]*Dept of Physics & Astronomy, Cardiff University, PO Box 913, Cardiff CF24 3YB*
[5]*Dipartimento di Astronomia, Universitá di Padova, Vicolo Osservatorio 5, I-35122 Padova, Italy*
[6]*Max-Planck-Institut für extraterrestrische Physik, PO Box 1603, 85740 Garching, Germany*
[7]*Institute for Astronomy, University of Edinburgh, Royal Observatory, Blackford Hill, Edinburgh EH9 3HJ*
[8]*Max-Planck-Institut für Astronomie, Königstuhl 17, D-69117 Heidelburg, Germany*
[9]*Institute of Astronomy, The Observatories, Madingley Road, Cambridge CB3 0HA*
[10]*Leiden University, PO Box 9513, NL-2300 RA Leiden, the Netherlands*
[11]*Institut d'Astrophysique Spatiale, Bâtiment 121, Université Paris XI, 91405 Orsay cedex, France*
[12]*Institut d'Astrophysique de Paris, 98bis Boulevard Arago, F 75014 Paris, France*
[13]*SISSA, International School for Advanced Studies, Via Beirut 2-4, 34014 Trieste, Italy*

Accepted 2000 March 17. Received 2000 March 13; in original form 1999 June 30

**ABSTRACT**

We present preliminary source counts at 6.7 and 15 μm from the preliminary analysis of the European Large Area *ISO* Survey, with limiting flux densities of ∼2 mJy at 15 μm and ∼1 mJy at 6.7 μm. We separate the stellar contribution from the extragalactic using identifications with automated plate measurement sources made with the likelihood ratio technique. We quantify the completeness and reliability of our source extraction using (a) repeated observations over small areas, (b) cross-identifications with stars of known spectral type, (c) detections of the point spread function wings around bright sources and (d) comparison with independent algorithms. Flux calibration at 15 μm was performed using stellar identifications; the calibration does not agree with the pre-flight estimates, probably due to effects of detector hysteresis and photometric aperture correction. The 6.7-μm extragalactic counts are broadly reproduced in the Pearson & Rowan-Robinson model, but the Franceschini et al. model underpredicts the observed source density by ∼0.5–1 dex, although the photometry at 6.7 μm is still preliminary. At 15 μm the extragalactic counts are in excellent agreement with the predictions of the Pearson & Rowan-Robinson, Franceschini et al., Guiderdoni et al. models and the evolving models of Xu et al., over seven orders of magnitude in 15-μm flux density. The counts agree with other estimates from the ISOCAM instrument at overlapping flux densities, provided a consistent flux calibration is used. Luminosity evolution at a rate of $(1 + z)^3$, incorporating mid-infrared spectral features, provides a better fit to the 15-μm differential counts than $(1 + z)^4$ density evolution. No-evolution models are excluded, implying that below around 10 mJy at 15 μm the source counts become dominated by an evolving cosmological population of dust-shrouded starbursts and/or active galaxies.

★ E-mail: s.serjeant@ic.ac.uk
† Current address: Astronomy Centre, Physics and Astronomy Subject Group, School of CPES, University of Sussex, Falmer, Brighton BN1 9QJ.

**Key words:** surveys – galaxies: evolution – galaxies: formation – galaxies: Seyfert – galaxies: starburst – infrared: galaxies.

## 1 INTRODUCTION

The *IRAS* mission enjoyed huge successes, including the sensational discoveries of ultra- and hyper-luminous galaxies and of an enormous population of evolving starbursts. However, the survey had several drawbacks. For example, the bright limiting flux densities restricted the samples to low redshifts ($z \lesssim 0.3$) for all but a few ultraluminous objects. Also, only ~1000 galaxies were detected at 12 μm over the whole sky. These deficiencies restricted the study of IR-luminous galaxies at all redshifts.

The *Infrared Space Observatory* (*ISO*) offered ~×1000 improvements in sensitivity in the mid-infrared over *IRAS*, and the large allocations of guaranteed and discretionary time for deep surveys on *ISO* will greatly improve on the *IRAS* surveys in the mid-infrared. For instance, *ISO* observations of the northern *Hubble Deep Field* (Serjeant et al. 1997, in preparation; Goldschimdt et al. 1997; Oliver et al. 1997; Aussel et al. 1999; Désert et al. 1999) reached the 15-μm confusion limit (~0.1 mJy) over 17 arcmin$^2$, while the CAM-Deep and CAM-Shallow surveys (Elbaz et al. 1998a,b) were slightly less sensitive but had wider areal coverage (0.5 mJy over 0.3 deg$^2$ and 0.8 mJy over 0.41 deg$^2$). These have also been complemented by deep *ISO* photometry of selected high-$z$ galaxies (e.g. Flores et al. 1999).

The European Large Area *ISO* Survey (ELAIS, Oliver et al. 1999 (Paper I); Rowan-Robinson et al. 1998) was the largest open time project on *ISO*, complementing the deep *ISO* samples by surveying ~12 deg$^2$ to a depth of ~2 mJy at 15 μm and ≲100 mJy at 90 μm. Around half the area was also mapped at 6.7 μm to ~1 mJy. Three fields in the northern hemisphere (N1, N2, N3) collectively comprised around two-thirds of the 15-μm areal coverage, with the remaining area taken by the southern S1 field and several small areas in both hemispheres. The ambitious cosmological aims include tracing the extinguished star formation history of the Universe to $z \sim 1$–2, orientation-independent selection of dust-shrouded quasars, and the potential discovery of hyperluminous galaxies (with comparable intrinsic luminosities to *IRAS* FSC 10214+4724) out to redshifts $z \lesssim 5$. A more detailed discussion of the diverse scientific aims of ELAIS, the selection of areas and observational parameters can be found in the ELAIS survey paper (Oliver et al. 2000); in summary, the survey areas were selected to have low galactic cirrus emission, high visibility by *ISO*, high ecliptic latitude and avoiding 12-μm *IRAS* sources brighter than 0.6 Jy. In another companion paper, Efstathiou et al. 1999, we discuss the 90-μm source counts from the preliminary analysis of the ELAIS ISOPHOT data, and in Crockett et al. (in preparation) we discuss the stellar mid-infrared source counts. The ELAIS areas have also been the subject of intensive multi-wavelength follow up, summarized to date in Oliver et al. (2000) and presented in detail in other papers (e.g. Ciliegi et al. 1999; Gruppioni et al. 1999). Here we present the completeness, reliability and extragalactic source counts from our initial preliminary 6.7 and 15-μm ISOCAM catalogues. A future paper will present the final analysis products from the ISOCAM ELAIS data, which is expected to improve on the preliminary analysis presented here.

This paper is structured as follows. In Section 2 we describe the preliminary analysis CAM pipeline, explaining the artefacts in the data (Section 2.1), and the pipeline algorithm (Section 2.2). The results from the preliminary analysis catalogue are presented in Section 3. Our various completeness and reliability estimates are discussed in Section 3.2, and the segregation of extragalactic from stellar sources in Section 3.3. Section 3.4 presents the source counts in both wavebands. These results are compared with source count models and previous results in Section 4, where we also discuss the implications for the evolution of star-forming galaxies and on the star-formation history of the Universe.

## 2 ELAIS CAM PRELIMINARY ANALYSIS

### 2.1 Data quality

The ELAIS CAM survey proper was conducted in raster mode (astronomical template CAM01), with the LW-2 (6.7 μm) and LW-3 (15 μm) filters. Details of the CAM01 Astronomical Observation Template (AOT) can be found in Paper I. The CAM detector is stepped across the sky in a grid pattern, with roughly half-detector-width steps in one direction and roughly whole detector widths in the other, covering approximately half a square degree per raster. This pattern leads to a redundancy of at least ×2 over most of the area surveyed. At each raster pointing (i.e. each grid position of the raster) the 32 × 32 CAM detector is read out several times.

Like the *ISO*-HDF North data (Serjeant et al. 1997, and in preparation; Aussel et al. 1999; Désert et al. 1999) the ELAIS CAM data contains many problematic artefacts (e.g. Lawrence 1996; Siebenmorgen et al. 1998). Because of the frequent and complicated glitches, we do not take the approach of reconstructing a sky map and searching for sources in these maps. Rather, we look for the characteristic signatures of sources and glitches in the time histories of individual pixels. See Starck et al. (1998) or Aussel et al. (1999) for more details.

The CAM detector also exhibits hysteresis. Source fluxes are initially around a factor of 2 fainter in instrumental units than the stabilized (i.e. asymptotic) value. Our survey strategy ensures that sources almost always have corroborating sightings in separate pixels. This permits a filter to remove glitch events from candidate sources.

### 2.2 Preliminary source extraction pipeline

#### *2.2.1 Preprocessing and deglitching*

The available CAM data reduction software underwent several substantial improvements over the lifetime of *ISO*, as the knowledge of the detector characteristics improved. However, from the outset we needed a method of preliminary data analysis, to feed for example immediate follow-up projects. Such a preliminary analysis pipeline may not of course represent best practice at the end of the *ISO* mission, but should at least provide a reasonably complete and reliable preliminary source list. It was decided that the CAM preliminary analysis data reduction should be as uniform as possible, which required that the preliminary analysis pipeline be fixed at an early stage. Accordingly our adopted pipeline could

not incorporate the accurate field distortion corrections (Abergel et al. 1998), which were not established at the start of the mission, nor the analytic models for the cosmic ray transients and detector hysteresis which were developed in the course of the *ISO* lifetime (e.g. Lari, in preparation; Abergel et al. 1998). Nevertheless, such improvements will be incorporated in future ELAIS final analysis products.

The data reduction was performed using the Interactive Data Language (IDL) software. The initial steps of the CAM Preliminary Analysis pipeline are straightforward. The edited raw data supplied by ESA were converted to IDL structures using the CAM Interactive Analysis (CIA, 1996 April version), and converted from ADUs (analogue-to-digital units) to ADUs per second. The default dark frame was subtracted from each exposure. To estimated the noise level in each pixel, we performed an iterative Gaussian fit to the histogram of readout values for each pixel. Cosmic ray spikes were then identified by $>4\sigma$ rises followed (one or two readouts later) by $>4\sigma$ falls. A similar algorithm was used to identify occasional readout troughs. The readout histograms were then re-fit and an empirical sky flat-field was obtained; the default ESA-supplied flat-field was found to give very unsatisfactory results. An attempt was made to model the initial detector stabilization using the Institut d'Astrophysique Spatiale (IAS) model within the CIA software package.

### 2.2.2 *Background estimation and source detection*

Unlike the detectors on the *IRAS* satellite (e.g. Neugebauer et al. 1984), the transients in the ISOCAM detector make the background levels in each pixel vary strongly and discontinuously with time. The approach adopted in the preliminary analysis was to estimate the background level in a given pixel and pointing from linear fits (in time) to the readouts in previous and subsequent pointings, then identify candidate sources from $>3\sigma$ features above the background in the pixel readout timelines. The source extraction pipeline is therefore spatially one dimensional. This simple approach avoids any explicit parametrizations of the transient profiles, which were not available at the time, and allows a local error estimate of the background level. This error was taken to be the formal error on the fit, but did not incorporate the instrumental noise at each data point. Since cosmic rays were frequently observed to cause discontinuities, the range for the linear fits extended no further than the nearest (in time) cosmic ray, and in any case not longer than three pointings. If an acceptable $\chi^2$ was not obtained in the linear fit, the range for the fit was decreased; if a good fit was still not obtainable, an average of the 10 nearest readouts was taken. Sources could then be identified from their excess above the extrapolated backgrounds. Since sources also create discontinuities, the data stream was iteratively re-fit treating $>3.5\sigma$ sources in the same way as cosmic rays above. An initial list of brightest sources was obtained before the iterative fitting, by searching for their discontinuous rise at the start of a pointing, and discontinuous fall at the end. Where sources were found (whether initially or in the iterative fitting) the background level in later iterations was extrapolated from only the previous pointings, ignoring the subsequent pointings, since the hysteresis after a source would otherwise lead to an overestimation of the background level. Sources were not extracted from the first or final pointings of the rasters, owing to limitations in the background fitting routines at the time the pipeline was frozen. Note that this iterative source extraction does not distinguish genuine sources from 'fader' transient events, so a further filter for source candidates is still required.

### 2.2.3 *Source corroboration*

The source detections in the pixel readout histories were spatially merged in each pointing using a connected pixel algorithm. (Note that there was no minimum number of pixel detections, unlike e.g. connected pixel source detection on an oversampled charge-coupled device image.) We then used the $\simeq\times2$ redundancy in the CAM rasters to search for corroborating observations of each source candidate. Genuine sources should be present in both observations, but glitch events should not be confirmed except by chance. The adopted search radius of two pixels, while large enough to safely encompass the (then uncertain) field distortion, nevertheless led to a large number of spurious detections, with the majority of source candidates at 15 μm being the result of glitch corroboration. Each candidate corroborated source was therefore examined by eye independently by at least two observers, who assigned quality flags of 1–4, where 1 refers to a 'definite source', 2 is a 'probable source', 3 'probably not' and 4 'definitely not'. Each raster in the LW-2 (6.7 μm) filter yielded typically $\sim$100 events in total of which around one half were classified as probable sources by at least one observer. In LW-3 (15 μm) both the number and fraction of spurious events was much higher: there were typically $\sim$30 strong source candidates, and a further 30–50 sources where the classification was ambiguous or debatable, with typically around 200–500 spurious events. Note that the preliminary analysis algorithm will necessarily miss sources with (a) only one observation or (b) corroborating observations in only the first or last pointings, so the effective area is slightly less than the nominal $\sim12\,\mathrm{deg}^2$.

### 2.2.4 *Astrometric corrections*

After the preliminary analysis reduction was complete, we improved the astrometry by incorporating the latest field distortion correction into the 15-μm source catalogues. Several sources with strong transient events nearby had their centroids strongly affected by the glitches. We therefore adopted a simple strategy for our preliminary analysis astrometry and flux calibration: the flux and (distortion-corrected) position of a source are taken from those of the brightest single-pixel detection of that source, excluding transients. We found this to be superior to (e.g.) masking nearby transients by eye then recalculating the centroids of the eyeball-accepted sources, particularly if the point spread function (PSF) wings lie on the detector, but the source itself is just outside. Our adopted algorithm should yield astrometry accurate to $\pm3$ arcsec in the absence of any other systematic errors. Two such systematics were expected in our data: first, errors in the position of the lens introduce a random astrometric offset to each raster of order one pixel; secondly, any errors in the calculation of the pointing position by CIA would offset any sources in that pointing. By examining the offsets with the likelihood-ratio identifications we can determine the lens offset empirically (Section 3.3). However, several rasters were found to have bimodal distributions of *ISO*-optical offsets, as a result of some unknown error in the CIA-derived astrometry in at least part of the raster. We therefore rederived the pointing astrometry using the ESA-supplied IIPH.FIT astrometry file, using the median coordinate positions in the duration of the pointing. This was found to remove the bimodality.

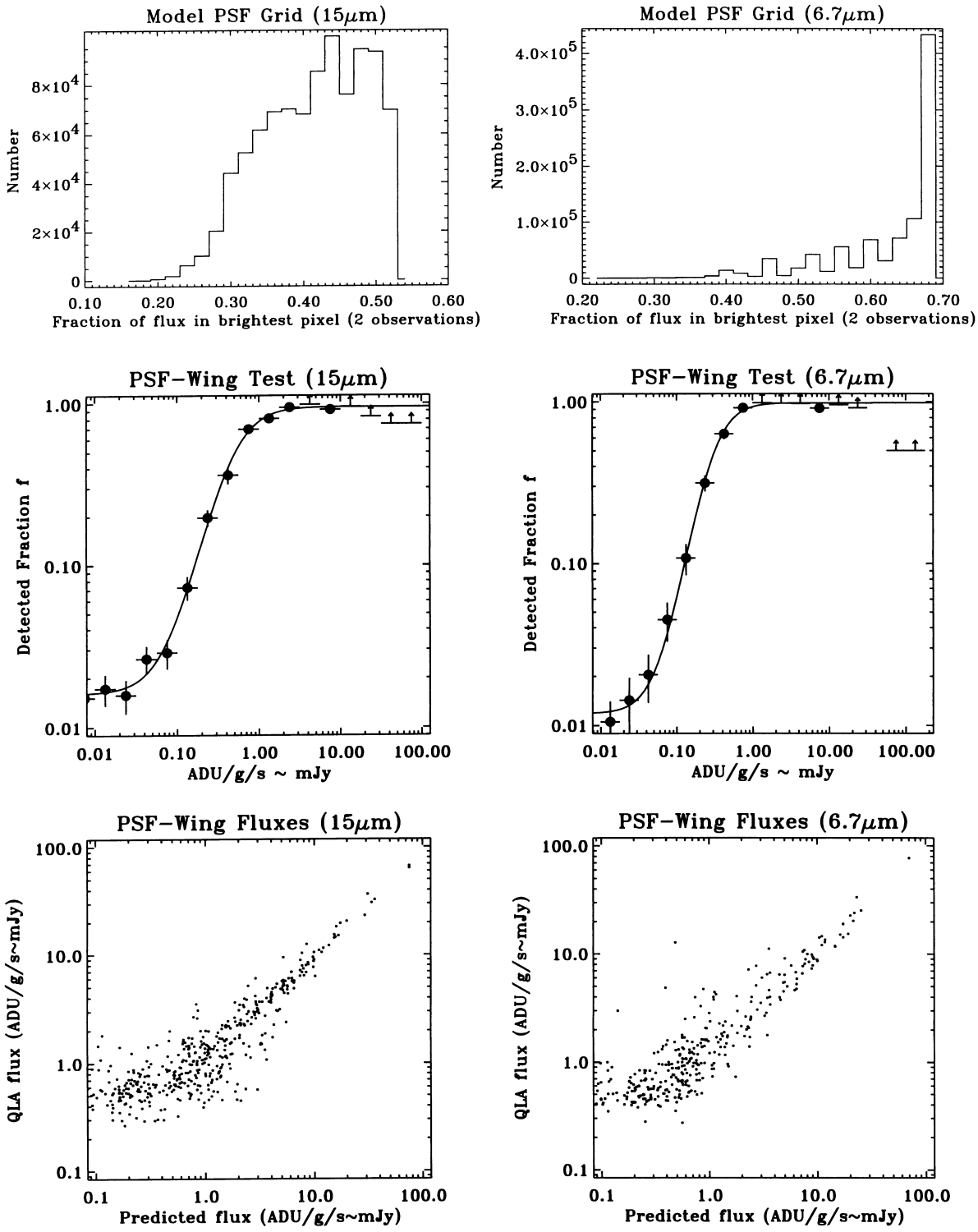


**Figure 1.** Panels show the 15 (left panels) and 6.7 μm (right panels) flux calibration data. Top panels show the distribution of the fraction of flux in the brightest (6 arcsec) pixel, out of *two* randomly placed observations of a point source. To calculate this, we use an evenly-spaced grid of theoretical PSF models from Aussel (private communication). The distribution is skewed to higher fluxes compared to the expected peak flux distribution of a single observation, and has smaller variance. The central panels show the detected fraction of individual pixels in the PSF wings of bright stellar sources. The central pixels in each star have been excluded from these plots. The lines show the best fit parametric model using equation (1). The lower panels show comparisons of the detected fluxes in individual pixels in bright point source PSF wings, with the predictions based on the PSF model. Again, the central pixels have been excluded from these plots.

#### 2.2.5 Aperture corrections to photometry

As discussed above, our source extraction method involves looking for characteristic time signatures in individual pixels. Without (at the time) a reliable and exact model for the glitch events, nor a reliable glitch event identification, we found that aperture photometry around our source positions was often seriously affected by nearby glitches. Instead of aperture photometry, we simply took the brightest flux of the pixels detecting the source, excluding (by eye) those pixels affected by glitches. Clearly, some aperture correction is needed to correct these peak pixel fluxes to total fluxes.

We can quantify these aperture corrections using a PSF model. In Fig. 1 we show the predicted flux in the brightest pixel of two randomly positioned observations of a point source (recall that at least two observations of a source are required for it to pass the preliminary analysis selection). At 15 μm, the brightest pixel has a flux of $\sim 0.4 \pm 0.1$ times the total flux of that source. At 6.7 μm the histogram is more sharply peaked, since the PSF is undersampled; the peak flux is always less than 0.69 times the total at 6.7 μm, but is greater than 0.5 (0.6) of the total in >90 per cent (>75 per cent) of occasions. We therefore applied global aperture corrections of 2.36 at 15 μm and 1.54 at 6.7 μm to our peak fluxes.

## 3 RESULTS

### 3.1 Eyeballing results

Our eyeballing results imply our catalogue is highly reliable to at least 3 mJy at 15 μm. In the ELAIS areas considered in this paper, there were 715 15-μm sources accepted by two observers, of which 510 had automated plate measurement (APM) identifications (Section 3.3); of the 816 singly-accepted sources at 15 μm, 212 had APM identifications. The singly-accepted sources are heavily skewed to faint fluxes: 90 per cent are fainter than 2.2 mJy. If we choose to regard all sources accepted by only one observer as false positives, and all sources accepted by two as true positives, then we obtain ∼80 per cent reliability for sources accepted by any observer at ∼3 mJy and ∼95 per cent at 5 mJy. These are one of the most pessimistic assumptions we could make; if alternatively we merge the doubly-accepted sources with the optically identified singly-accepted sources, the reliability (fraction doubly-accepted) of the sources accepted by any observer rises to ∼95 per cent at ∼3 mJy and increases at brighter fluxes. The blank-field singly-accepted sources are heavily skewed to faint fluxes, so we can neglect their effect on the counts above 3 mJy and combine the doubly-accepted sources with the optically identified singly-accepted for the purposes of the source counts. However this is not to say that the fainter singly-accepted sources necessarily have lower reliability, since the genuine fainter sources may have fainter optical counterparts. The situation is similar at 6.7 μm. Of the singly-accepted sources 95 per cent have fluxes less than 1.5 mJy.

### 3.2 Completeness, reliability and flux calibration

#### 3.2.1 Repeated observations

There are several potential approaches to estimating the Preliminary Analysis completeness and reliability, the most obvious of which is repeated observations over small areas. Oliver et al. (2000) present 10 repeat observations of a small ELAIS raster, covering at least six known sources by design. The source extractions in the individual reductions confirmed our result that the source extraction is highly complete and reliable at flux densities above ∼2.5 mJy at 15 μm.

#### 3.2.2 PSF-wing test

One robust test of our temporal source extraction is to examine the point spread function wings of bright sources. Like the cross-correlation with bright stars, this relies on the knowledge that a given pixel is illuminated by a known source flux, but has the advantage that the comparison can be taken to arbitrarily faint flux levels. We selected the 30 brightest 15-μm sources with stellar optical identifications, and selected a model theoretical PSF (Aussel, private communication) with the smallest rms difference in the central $3 \times 3$ PSF pixels. We normalized the PSF to the source flux using the mean observed flux in the central pixel. Using this model we predicted the mean flux in each pixel of the PSF wings, and hence determined the single-pixel detection efficiency $f$ of the temporal source extraction. The results are shown in Fig. 1. We can also compare the predicted PSF fluxes with the fluxes extracted by the preliminary analysis algorithm, shown in Fig. 1. The relation is encouragingly linear, although the scatter is larger than expected (by ∼×2 at 15 μm) based on the quoted errors in the preliminary analysis sky background fits. This is perhaps not surprising, since the background fitting algorithm does not make use of the detector noise in the fit, so will tend to underestimate the background-level uncertainty; also, non-white-noise features may prevent the noise scaling as $\sqrt{N}$. Oddly, the discrepancy in the scatter is largest at brightest fluxes. Plausible explanations include slight errors in the source centroids or in the theoretical PSF shape, both of which sensitively affect the brightest flux predictions. Analogous results for the 30 brightest 6.7-μm stars are also shown in Fig. 1. The undersampling of the PSF at 6.7 μm makes the scatter harder to interpret: more of the flux is contained in the central pixel making it less sensitive to errors in the assumed PSF shape, but is more affected by the much larger uncertainty in the centroid.

There are several caveats which apply to the high apparent completeness in Fig. 1. The chance detections of 'faders' will tend to increase this estimate, but since both the 6.7 and 15-μm completeness appear to asymptote to ∼0.015 (i.e. probability of detection of nearby spurious events is 1.5 per cent) this appears not to be a serious problem. This is also only applicable to single-pixel detections, whereas in fact the CAM detector Nyquist samples the PSF at 15 μm. Indeed at 15 μm the fraction of the flux in the brightest pixel rarely exceeds 0.5 although the same does not apply at 6.7 μm. The completeness also is not the detected source fraction $F$ but rather $F^2$, since we require at least two independent detections for a source to be accepted by our algorithm. There is also a slight bias in that the brightest detected sources are not typically observed when the detector is suffering the strongest transients, because the sources would not otherwise be detected. Finally, any incompleteness caused by the eyeballing, or by any areal coverage lost to e.g. cosmic ray impacts, would not be included in these estimates as they stand.

We can therefore estimate the preliminary analysis completeness from the PSF-wing test in the following way. We can convolve the single-pixel detection rate in Fig. 1 with the peak flux distribution expected from the PSF models to obtain the source sensitivity $F$ for single observations. The preliminary analysis completeness, before eyeballing, will then be proportional to $F^2$,

assuming the PSF wings themselves are representative of the data as a whole.

We fit the detected fractions in Fig. 1 with tanh functions, i.e.

$$f(S) = \frac{(f_{\max} - f_{\min})}{2} \tanh(\alpha \log_{10}(S/S_0) + 1) + f_{\min}, \quad (1)$$

where $f_{\min}$ and $f_{\max}$ represent the asymptotic limits at faint and bright fluxes respectively. We define the single-pixel source detection fraction to be $f'(S) = f(S) - f_{\min}$, and use a grid of PSF models (each normalized to 1) spanning the possible range of centroid positions to estimate the single-pointing source detection:

$$F(S) = \frac{1}{N} \sum_{i=1}^{N} f'(S \times S_{\mathrm{peak},i}), \quad (2)$$

where $S_{\mathrm{peak},i}$ is the peak flux in the $i$th PSF. This assumes that if a source is not detected in the peak pixel, it will not be detected in any pixel. The maximum areal coverage of the preliminary analysis, i.e. excluding the first and last pointings of each raster and regions with no redundancy, is $\Omega_{\max} = 10.0\,\mathrm{deg}^2$ at 15 μm, and $\Omega_{\max} = 6.51\,\mathrm{deg}^2$ at 6.7 μm. From this we obtain the preliminary analysis areal coverage as a function of flux:

$$\Omega_{\mathrm{preliminary\ \ analysis}}(S) = \Omega_{\max} F^2(S). \quad (3)$$

The final areal coverage from the PSF-wing test is plotted in Figs 2 and 3.

### 3.2.3 *Comparison with IAS and CEA pipelines*

As a final check of the completeness of our preliminary analysis catalogue, we compared our source extraction in the repeat observation regions (cf. Oliver et al. 2000 and Section 3.2.1) with extractions made with the CAM-Deep pipeline developed at the Commisariat á L'Energie Atomique, Saclay (CEA; Baker, private communication) and a pipeline based on the 'Triple Beamswitch' method developed at Institut d'Astrophysique Spatiale (IAS; Clements, private communication; Désert et al. 1999). Of our six robust sources (Section 3.2.1), CEA and IAS both identify three (the same three), with fluxes brighter than ∼3 mJy. This appears to be mainly because the preliminary analysis pipeline extracts lower signal-to-noise sources, but supplements with greater manual eyeballing. Nevertheless, this confirms that we are not significantly underestimating the surface density of sources brighter than 3 mJy.

### 3.2.4 *Flux calibration and cross-correlation with bright stars*

Another useful test of the completeness is to search for detections at the locations of bright stars (see Section 3.3 for details of the optical identification algorithm). If the spectral types of the stars are known, one can predict their mid-infrared fluxes. An exception would be dust-shell stars, but these are expected to be rare in the survey. In Crockett et al. (in preparation) and Crockett (in preparation) the sources are cross-correlated with stars from the Simbad and *Hipparcos* data bases. All 22 stars with predicted fluxes brighter than 3 mJy at 15 μm were detected in the preliminary analysis, and all but two of the 20 stars with predicted 6.7-μm fluxes above 1 mJy appeared in the preliminary analysis. To assess the level of random associations, we randomized the stellar positions within the ELAIS fields and repeated the cross-association, and found none. The 15-μm completeness is shown in Fig. 4. Note that this is an extremely robust estimator of the completeness, since the stellar flux prediction algorithm reproduces *IRAS* fluxes well, and the stars cannot be argued to lie on atypical regions of the detector.

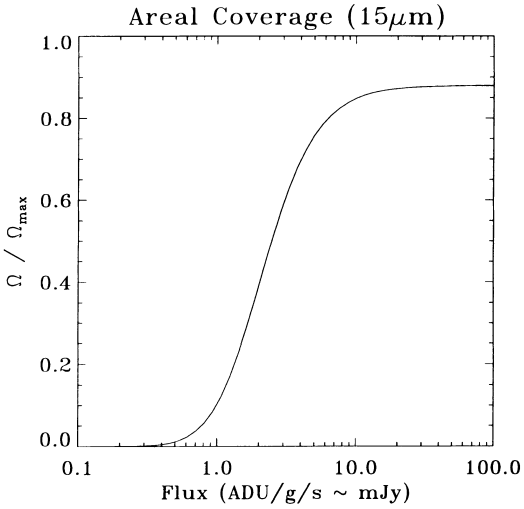


**Figure 2.** Effective areal coverage in the LW-3 15-μm band. The maximum coverage, which excludes the first and last pointings of each raster and regions without redundancy (removing 7 per cent from each raster), is $\Omega_{\max} = 10.0\,\mathrm{deg}^2$. The curves asymptote to <1 because the bright end of the PSF-wing test is not well constrained, having only a few weak limits. Also the asymptotic value at low fluxes is not included (and is also ill-constrained) since this is presumably glitch confirmation.

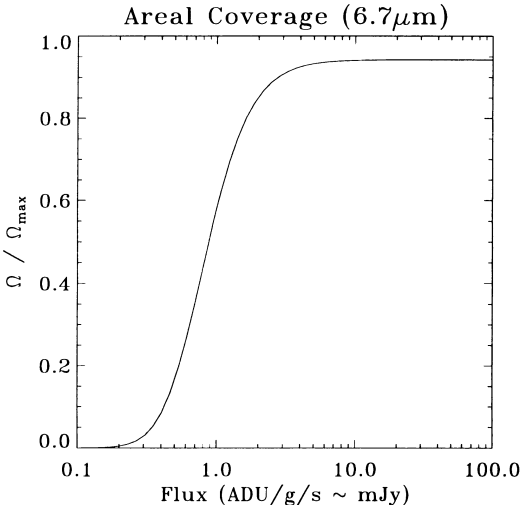


**Figure 3.** Effective areal coverage in the LW-2 6.7-μm band. The maximum coverage, which excludes the first and last pointings of each raster and regions without redundancy (removing 7 per cent from each raster), is $\Omega_{\max} = 6.51\,\mathrm{deg}^2$.

However, the flux calibration implied by these associations is around a factor of 2 discrepant with the expectation that ADU $\mathrm{gain}^{-1}\,\mathrm{s}^{-1} \simeq$ mJy at 15 μm (see Fig. 5). Across the entire range in flux, the $\pm 1\sigma$ limits on the log of the calibration ratio are $0.246 \pm 0.050$, i.e. the ratio is $1.75^{+0.26}_{-0.23}$. As shown in Fig. 5, there are hints that this calibration is a function of flux, with a calibration ratio of 2 preferred at faint fluxes (where indeed most of our sources lie). (The ISOCAM Observer's Manual (ISOCAM Consortium 1994) recommends a conversion of approximately 2 ADU $\mathrm{gain}^{-1}\,\mathrm{s}^{-1}$ to 1 mJy at 15 μm for fully stabilized sources,

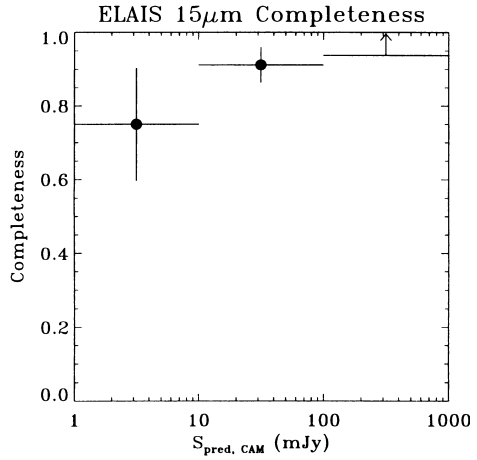


**Figure 4.** Completeness at 15 μm estimated from the predicted fluxes of stars in the main ELAIS regions. For more details see Crockett et al. (in preparation).

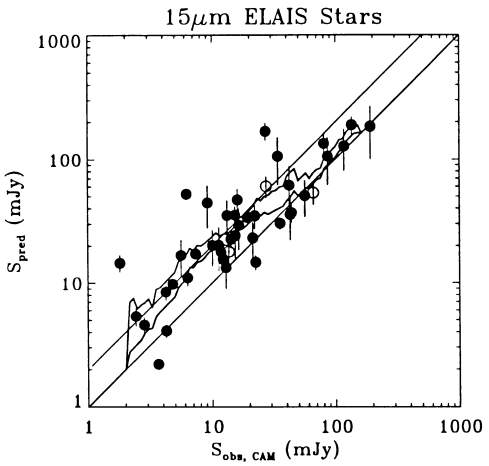


**Figure 5.** Flux calibration at 15 μm estimated from the predicted fluxes of stars in the main ELAIS regions. The observed fluxes assume a one-to-one conversion between ADU gain$^{-1}$ s$^{-1}$ and mJy. Open points are from *Hipparcos*, and solid points from Simbad. As discussed in Crockett et al. (in preparation), the most reliable spectral typing and hence mid-infrared predictions are available for Simbad stars. The straight lines show a 1:1 and 2:1 ratio between observed and predicted counts. Also shown is the $\pm 1\sigma$ limits on the mean observed:predicted ratio as a function of flux, calculated within $\pm 0.25$ dex of each flux (i.e. an 0.5 dex boxcar smoothing). There are perhaps hints from this figure that the flux calibration may be a weak function of flux, although in this paper we assume a flux-independent scaling. For more details see Crockett et al. (in preparation) and Misoulis et al. (1998).

and after correcting for the loss of flux resulting from a lack of stabilization (e.g. Section 2.1), becomes approximately a 1:1 conversion.) To predict the fluxes we followed the procedure of Crockett et al. (in preparation) and Misoulis et al. (1998), incorporating the passband profiles (for more details we refer the reader to these papers; the algorithm accurately reproduces stellar mid-infrared *IRAS* fluxes so there are unlikely to be significant systematics in the CAM-flux predictions). It is not immediately clear what might cause such a discrepancy, although there are several possibilities, such as the uncertainties in the PSF for the aperture correction, and the assumed ~×2 loss in flux (Section 2.1) from the lack of an upward source stabilization correction. (Note that differences in the PSF due to the differing spectral slopes of the stars are too small to account for the discrepancy: e.g. Aussel et al. (1999) find it only to be a ~10 per cent effect.) For the purposes of the source counts we will adopt the mJy : ADU gain$^{-1}$ s$^{-1}$ = 1 : 2 stellar calibration implied in Fig. 5, where the ADUs are not corrected for losses due to lack of stabilization.

At 6.7 μm a lower bound of 95 per cent can be made on the completeness at fluxes >10 mJy, but the uncertain aperture corrections make applying the stellar flux calibration more difficult. As a preliminary measure we therefore simply take the pre-flight ISOCAM Observer's Manual (ISOCAM Consortium 1994) calibration at 6.7 μm, corrected by a factor ~2 (Section 2.1) to account for the loss in flux from lack of stabilization.

In summary, our various completeness estimates yield a ⩾1 mJy limit to the completeness at 15 μm, and ⩾0.5 mJy at 6.7 μm (Figs 2 and 3) using the ISOCAM Observer's Manual (ISOCAM Consortium 1994) flux calibration corrected by a factor of 2 to account for stabilization loss (Section 2.1). However our stellar cross-correlation suggests we have underestimated the fluxes by a factor of ~2 at 15 μm (Fig. 5) so the 15-μm completeness quoted should by revised upwards to ⩾2 mJy. In *all* subsequent discussion, the 15-μm ELAIS fluxes are assumed to obey this stellar flux calibration.

### 3.3 Optical identifications

In this section we summarize the optical identification algorithm used for the preliminary analysis catalogue, for APM stars and galaxies (McMahon & Irwin 1992). We adopted the likelihood-ratio procedure of Sutherland & Saunders (1992) to associate our preliminary analysis sources with known objects. The surface density of catalogue objects as a function of magnitude is incorporated into the likelihood of each identification of the preliminary analysis sources with the catalogue objects. Following Mann et al. (1997), we define the likelihood ratio to be the ratio of the probability of detecting a genuine counterpart to the source with the position and flux of the catalogue object, to the probability of such an association occurring by chance given the positional errors. For a catalogue surface density $n(f)$ (where $f$ is the flux), a positional uncertainty $\epsilon(x, y)$ (where $x$ and $y$ are e.g. Cartesian coordinates) and an a priori flux distribution of IDs given by $q(f)$, the likelihood ratio is given by

$$LR(f, x, y) \propto \frac{q(f)\epsilon(x, y)}{n(f)}. \quad (4)$$

Using this expression and, assuming $q(f)$ to be constant as a function of optical magnitude, we found, for each preliminary analysis source, the object in the APM catalogue giving the highest likelihood ratio. We normalized the likelihood ratios by finding the maximum likelihood-ratio associations around random source positions, to yield probabilities for each preliminary analysis identification, and accepted identifications with random probabilities of less than 0.3. Slight errors in the lens positioning lead to systematic astrometric shifts in each raster, of order a few arcseconds. To correct for this, the high-likelihood identifications in each raster were used to determine any systematic astrometric offset. The identifications were subsequently rederived. There were not enough reliable optical identifications to obtain a robust estimate of the lens offset in the smaller ELAIS areas, so the

analysis was restricted to the main ELAIS areas of N1, N2, N3 and S1. Further discussion of the identifications is deferred to later papers in this series.

### 3.4 Source counts

Using the completeness and reliability from Section 3.2, we can extract the extragalactic source counts at 6.7 and 15 μm. For the purposes of the counts we included all sources accepted by (at least) two observers. From this list, we exclude 15-μm stellar identifications brighter than approximately $B = 16.5$ (assuming a monotonic stellar plate saturation correction converting $B = 18$ galaxy magnitudes to $B \lesssim 16.5$ stars), but include fainter stellar IDs since these are expected to be predominantly active galactic nuclei (AGN). All stellar IDs at 6.7 μm were eliminated from the extragalactic source counts. It is highly unlikely for stars with $B > 16.5$ to be detected at 15 μm to these limits ($B = 16.5$ is equivalent to $S_B = 1$ mJy; see also Crockett et al., in preparation; Crockett, in preparation), with the exception of rare dust-shell stars. Note also that all the 15-μm (6.7-μm) sources accepted by only one observer are fainter than 2.2 mJy (2.5 mJy), so we can be highly confident of the reliability of sources brighter than these limits.

The segregation of extragalactic from stellar counts is robust at 15 μm, but the large fraction of stellar IDs at 6.7 μm make it possible that some faint stars have been included in the extragalactic counts at this wavelength: of the 794 doubly-accepted sources at 6.7 μm, only 79 have stellar APM classifications faint enough to be accepted in the extragalactic counts. We eyeballed the Digitized Sky Survey (DSS) images of every optical identification of the 6.7 and 15-μm sources. We found the by-eye classifications to agree with the APM in nearly all cases. The

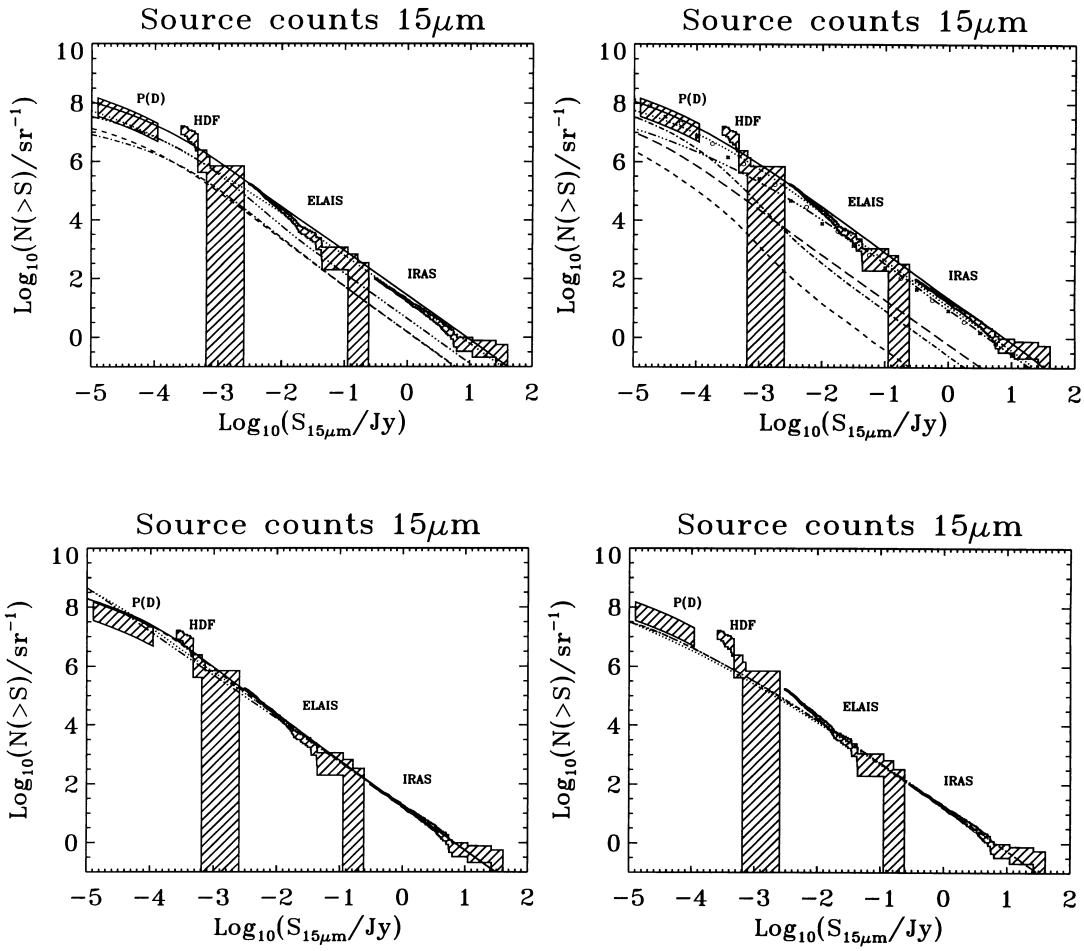


**Figure 6.** Integral ELAIS extragalactic source counts at 15 μm. Flux densities are quoted in Jy. Shaded regions show the ranges spanned by $\pm 1\sigma$ uncertainties. Also shown are the source counts and P(D) analysis from the *Hubble Deep Field* (Oliver et al. 1997; Aussel et al. 1999). The *IRAS* counts are estimated from the 12-μm counts as discussed in the text. Top left panel shows the Pearson & Rowan-Robinson (1996) model. Dotted line shows normal galaxies, dashed line shows Seyfert I galaxies, dot-dashed are Seyfert IIs, and starbursts are dash-dot-dot-dot. The total is shown as a full line. Top right panel shows the Franceschini et al. (1994) source count model overplotted. The model spiral contribution is shown as a dotted line, ellipticals as a dashed line, S0 as a dash-dot line, starbursts as a dash-dot-dot-dot line and AGN as a long dashed line. The total population model is shown as a full line. Also plotted are the Guiderdoni et al. (1997) models A and E, as small filled crosses and small open circles respectively. Bottom left panel shows the evolving Xu et al. (1998) models, renormalized by ×1.8 to match the *IRAS* counts as in Fig. 6. The full line shows $(1+z)^3$ luminosity evolution with K-corrections derived from starburst models with mid-infrared features, and the dashed line shows the same luminosity evolution without the mid-infrared features. Density evolution of $(1+z)^4$ with mid-infrared features is plotted as a dotted line, and without mid-infrared features as a dash-dot-dot-dot line. Bottom right panel shows all available no-evolution models. Franceschini et al. (in preparation) is overplotted as a dash-dot-dot-dot line. The Xu et al. (1998) models are shown with and without the mid-infrared spectral features (dash-dot and dotted respectively). All three no-evolution models have been renormalized to match the *IRAS* counts, by a factor of 0.8 for the Franceschini et al. models, and 1.8 in the case of the Xu et al. (1998) models.

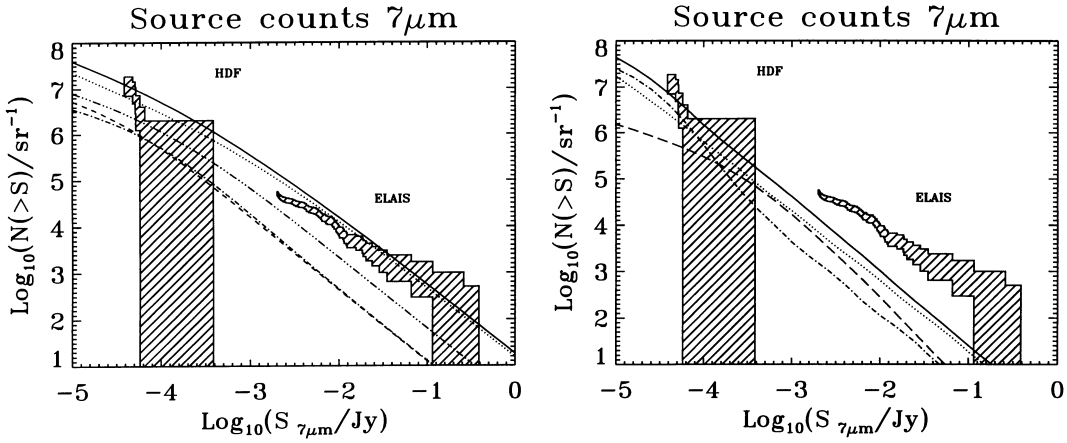


**Figure 7.** Preliminary integral ELAIS extragalactic source counts at 6.7 μm, using the flux calibration discussed in the text. Flux densities are quoted in Jy. Left panel shows the Pearson & Rowan-Robinson model overplotted, and right panel shows the Franceschini et al. (1997) model. Symbols as in the respective panels of Fig. 6.

resultant extragalactic counts are virtually indistinguishable from the automated segregations at both 6.7 and 15 μm.

The extragalactic source counts are plotted in Fig. 6, using the by-eye star-galaxy separation and the stellar flux calibration. The 15-μm Lockman Hole ISOCAM survey data will be discussed in Elbaz et al. (1999). The counts from this survey at around the ∼5 mJy level, which overlap with the ELAIS counts, appear significantly lower than those of ELAIS. However this is entirely attributable to the ∼×2 differences in assumed flux calibration. The counts are in excellent agreement in instrumental units or in mJy with the same flux calibration assumption; alternatively, a ∼30 per cent reduction of the ELAIS preliminary analysis 15-μm flux calibration factor would also bring the counts into formal $1\sigma$ agreement while remaining consistent with Fig. 1. However this may require a commensurate reduction in the *IRAS* counts. Such a reduction has been argued to be necessary by Elbaz et al. (1999) in order to account for large-scale-structure effects in the Rush, Malkan & Spinoglio (1993) sample.

Also plotted are the 12-μm source counts calculated by Oliver et al. (1997) from the Rush et al. (1993) sample, using the QMW *IRAS* Galaxy Mask (Rowan-Robinson et al. 1991), and transposed to 15 μm assuming a population mix matching the Pearson & Rowan-Robinson (1996) predictions. The faint source counts from the *ISO*-HDF North survey (Oliver et al. 1997) are also shown in the counts figures. The ELAIS extragalactic preliminary analysis counts at 15 μm are consistent with an interpolation between the *ISO*-HDF North and Rush et al. (1993) data sets, and at 6.7 μm with reasonable extrapolations from the *ISO*-HDF North. The source density at 15 μm is also in good agreement with that obtained at 12 μm by Clements et al. (1999), although the differing K-corrections do not make it immediately clear that the counts must necessarily agree (e.g. Xu et al. 1998; Serjeant 1999). Note that the 6.7-μm counts have significant photometric errors independent of flux, owing to the undersampling of the PSF (Fig. 1). For a constant source count slope the shape of the counts is unaffected by flux-independent errors, so we can regard the 6.7-μm counts as subject to a potential systematic error in the form of a horizontal shift. Such a systematic is less than or of order a factor 2 in flux. We overplot the model predictions from Pearson & Rowan-Robinson (1996) in Figs 6 and 7, as well as the model predictions of Franceschini et al. (1994, 1997). Also overplotted are the Guiderdoni et al. (1997) 15-μm model counts and the evolving models from Xu et al. (1998), with and without mid-infrared spectral features. Note that all the Xu et al. models have been renormalized to match the *IRAS* counts. Fig. 6 also compares the observations to a variety of non-evolving models. Apart from the renormalization to the *IRAS* Rush et al. (1993) × QIGC counts, these are the same non-evolving models as discussed in Elbaz et al. (1998a,b).

## 4 DISCUSSION

The experimental agreement with the evolving models of Pearson & Rowan-Robinson (1996), Franceschini et al. (1994), Guiderdoni et al. (1997) and Xu et al. (1998) at 15 μm over seven orders of magnitude in flux density is striking. The starbursts in the Pearson & Rowan-Robinson (1996) models are normalized to the 60-μm *IRAS* counts, but not explicitly to the 12-μm counts. The slight overprediction of the *IRAS* counts is also present in the ELAIS counts, until a slight upturn at around 10 mJy (which is not an effect of incompleteness or low reliability), departing from the Euclidean slope, brings the data into closer agreement with the model. Of the four Xu et al. (1998) models, the $(1+z)^3$ luminosity evolution models have the stronger upturn, reproducing the observed counts slightly more well than the alternative $(1+z)^4$ density evolution. This is clearer still in the 15-μm differential counts (Fig. 8), where luminosity evolution is shown to make a much better fit to the ELAIS counts, although an even larger excess is suggested by the *ISO*-HDF counts. Note that we renormalized the Xu et al. (1998) predictions by ×1.8 to match the *IRAS* counts.

The source count models present rather different predictions at 6.7 μm. The Pearson & Rowan-Robinson (1996) model has only a slight overestimate, accountable for instance to the flux calibration uncertainties. However, the underprediction in the Franceschini et al. (1997) model is over an order of magnitude, probably too large to be an artefact of our albeit uncertain flux calibration at this wavelength. This discrepancy is most likely to be due to deficiencies in the assumed spectral energy distributions, which are not well-constrained in this wavelength range (e.g. Serjeant 1999), rather than the result of incorrect assumptions about the evolution or population mixes.

The loss of the *Wide Field Infrared Explorer* (*WIRE*) satellite

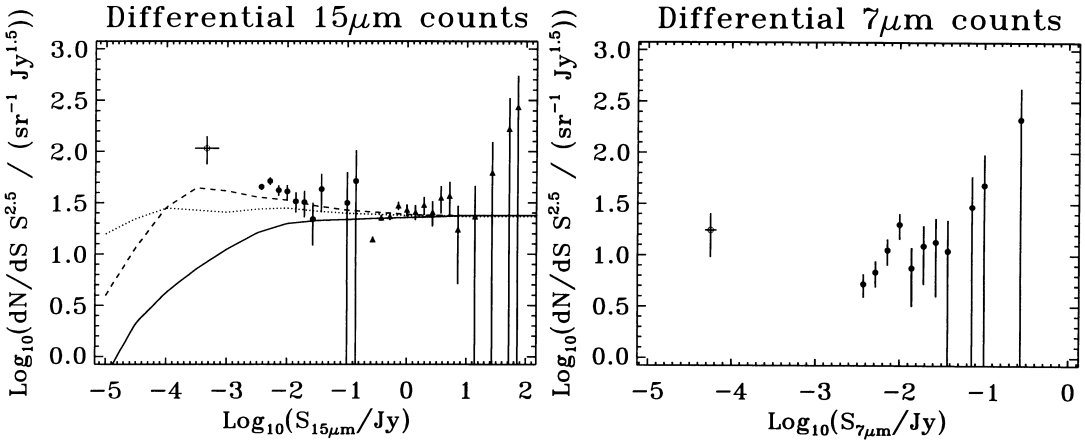


**Figure 8.** Left panel shows Euclidean-normalized differential source counts at 15 μm. Flux densities are quoted in Jy. Triangles show the Rush et al. (1993) sample, and filled circles show ELAIS. The open circle is taken from the *ISO*-HDF sample (Oliver et al. 1997). The filled line is the no-evolution model of Xu et al. (1998) with mid-infrared spectral features incorporated. The dotted and dashed lines respectively show the Xu et al. (1998) predictions for $(1+z)^3$ pure luminosity evolution and $(1+z)^4$ pure density evolution, both including mid-infrared spectral features. All three Xu et al. (1998) models have been renormalized by $\times 1.8$ to match the *IRAS* counts. Horizontal error bars (where shown) indicate the width of the flux bins for the fainter samples, and vertical error bars the $\pm 1\sigma$ Poisson errors on the counts. The right panel shows Euclidean-normalized differential source counts at 6.7 μm. Flux densities are quoted in Jy. Filled circles show ELAIS, and the open circle shows the *ISO*-HDF sources (Oliver et al. 1997) with optical IDs.

was a serious blow to infrared extragalactic astronomy. In the hope or expectation of a new *WIRE* mission, we can compare our source counts with the expectations of the *WIRE* team. *WIRE* was to survey at least 170 deg$^2$ to a limiting 12-μm sensitivity of 1.9 mJy, and smaller areas to deeper limits. Our source counts imply a surface density of approximately 100 galaxies per square degree to the projected *WIRE* 12-μm bright survey limit, using the Pearson & Rowan-Robinson or Franceschini et al. 15-μm source count models to extrapolate. This is larger than the projected source density of the *WIRE* team (q.v. Fig. 6, bottom-right panel, and 8 left panel, where the *WIRE* predictions were renormalized upwards by a factor of ∼2 to match, e.g. the observed *IRAS* and ELAIS counts). Although encouraging for the numbers of sources, it suggests that surveys much deeper than this will very rapidly be confusion limited. This is in good agreement with the observations of Oliver et al. (1997). The composite counts from the various 15-μm surveys also imply that confusion will be irrelevant, e.g. for the Next Generation Space Telescope (NGST), but will be significant for the MIPS imager on the Space Infrared Telescope Facility (SIRTF) even in short (∼2000 s) exposures. The gains in detector size and sensitivity in future missions will offer very large improvements in wide-field survey efficiency: for example, a survey of a similar depth and areal coverage to ELAIS at 15 μm will be possible with MIPS on SIRTF in only ∼10 h.

The upturn in the counts at faint fluxes continues in the *Hubble Deep Field ISO* counts, and is too large to be attributable to starburst K-corrections (e.g. Xu et al. 1998; Elbaz et al. 1998a,b). This excess is above any reasonable no-evolution predictions (Fig. 6), which all have shallower slopes than the evolving models independent of K-correction and world models. This implies that the faintest sources in ELAIS are sampling a significantly cosmologically evolving mid-infrared population. Given the strong evolution in both the comoving star formation rate claimed from optical–UV observations and in the quasar comoving number density, as well as the large fraction of AGN and starbursts expected in ELAIS from the counts models, we can reasonably expect that optical spectroscopy of ELAIS and fainter samples will have a major impact on the study of dust-shrouded star formation and quasar activity and their evolution. The prediction from the Pearson & Rowan-Robinson (1996) source count models is for of order of a few objects as (intrinsically) luminous as *IRAS* F10214+4724 out to $z = 4$ over the entire ELAIS areas. The mid-infrared luminosity function and luminosity density can be used to derive a comoving star formation rate without the difficult problems of extinction corrections that affect optical–UV estimates, and (for the ISOCAM LW3 filter) is reasonably free of K-correction uncertainties (Xu et al. 1998; Serjeant 1999). The ELAIS survey is also highly sensitive to obscured quasars and will be an exceptional resource for active galaxy unification models. The ELAIS limits can also provide important constraints for sources detected at other wavelengths: for example, the 15, 90 and 175 μm limits at 850-μm source positions can provide robust redshift constraints (e.g. Hughes et al. 1998).

## 5 CONCLUSIONS

The extragalactic source counts agree extremely well with all evolving model predictions (Franceschini et al. 1994; Pearson & Rowan-Robinson 1996; Guiderdoni et al. 1997; Xu et al. 1998) over seven orders of magnitude in 15-μm flux density. The Pearson & Rowan-Robinson (1996) models can broadly reproduce the 6.7-μm extragalactic counts, but the observations are in excess of the Franceschini et al. (1997) predicted counts at this wavelength using our preliminary 6.7-μm flux calibration. All no-evolution models are clearly excluded, and imply a cosmologically evolving population of obscured starbursts and/or active galaxies dominant below ∼10 mJy at 15 μm, independent of K-correction assumptions. Source confusion appears to have been underestimated in the *WIRE* and SIRTF missions, but will not impact significantly on the NGST.

## ACKNOWLEDGMENTS

We would like to thank Dave Alexander and Ruth Carballo for helpful comments and proof reading of this paper. This paper is

based on observations with *ISO*, an ESA project with instruments funded by ESA member states (especially the PI countries: France, Germany, the Netherlands and the United Kingdom) and with participation of ISAS and NASA. The ISOCAM data presented in this paper was analysed using 'CIA', a joint development by the ESA Astrophysics Division and the ISOCAM Consortium. The ISOCAM Consortium is led by the ISOCAM PI, C. Cesarsky, Direction des Sciences de la Matiere, C. E. A., France. This work was supported by PPARC (grant number GR/K98728) and by the EC TMR Network programme (FMRX-CT96-0068).

## REFERENCES

Abergel A. et al., 1998, ISOCAM Interactive Analysis User's Manual version 3.0, SAI/96-5226/Dc
Aussel H., Cesarsky C. J., Elbaz D., Starck J. L., 1999, A&A, 342, 313
Ciliegi P. et al., 1999, MNRAS, 302, 222
Clements D., Désert F.-X., Franceschini A., Reach W. T., Baker A., Davies J. K., Cesarsky C., 1999, A&A, 346, 383
Désert F. X., Puget J. L., Clements D. L., Pérault M., Abergel A., Bernard J.-P., Cesarsky C. J., 1999, A&A, 342, 363
Elbaz D. et al., 1998a, in Cox P., Kessler M. F., eds, The Universe as seen by ISO, ESA Special Publications Series (SP-427), UNESCO, Paris, astro-ph/9902229
Elbaz D., Aussel H., Cesarsky C. J., Desert F. X., Fadda D., Franceschini A., Puget J. L., Starck J. L., 1998b, Proc. of 34th Liege International Astrophysics Colloquium on the Next Generation Space Telescope, astro-ph/9807209
Elbaz D. et al., 1999, astro-ph/9910406
Flores H. et al., 1999, ApJ, 517, 148
Franceschini A., Mazzei P., de Zotti G., Danese L., 1994, ApJ, 427, 140
Franceschini A. et al., 1997, in Wilson E., ed., Proc. of the ESA Symp. The Far Infrared and Submillimeter Universe. ESA Special Publications ESA SP-401, UNESCO, Paris, p. 159–167
Goldschmidt P. et al., 1997, MNRAS, 289, 465
Gruppioni C. et al., 1999, MNRAS, 305, 297
Guiderdoni B., Hivon E., Bouchet F. R., Maffei B., 1997, in Bouchet F. R., Gispert R., Guilderdoni B., Tran Thanh Van J., eds, Microwave Background Anistropies: Proc. of the XVIth Moriond Astrophysics Meeting. Editions Frontieres, Gif-sur-Yvette
Hughes D. et al., 1998, Nat, 394, 241
ISOCAM Consortium, 1994, ISOCAM Observer's Manual version 1.0. ESA/ESTEC, Noordwijk, The Netherlands
Lawrence A., 1996, Character of Glitches in the First ISOCAM Raster, ELAIS Technical Note
Mann R. G. et al., 1997, MNRAS, 289, 482
McMahon R. G., Irwin M. J., 1992, in MacGillivray H. T., Thomson E. B., eds, Digitised Optical Sky Surveys, Astrophysics and Space Science Library, Vol. 174. Kluwer, Dordrecht, p. 417
Misoulis V., Crockett H., Oliver S., Dapergolas A., Serjeant S., Rowan-Robinson M., Kontizas E., Kontizas M., 1998, in Cox P., Kessler M. F., eds, The Universe as seen by ISO, ESA Special Publications Series (SP-427), UNESCO, Paris
Neugebauer G. et al., 1984, ApJL, 278, 1
Oliver S. et al., 1997, MNRAS, 289, 471
Oliver S., Gruppioni C., Serjeant S., 1998, MNRAS, submitted (astro-ph/9808260)
Oliver S. et al., 2000, MNRAS, 316, 749 (Paper I, this issue)
Pearson C., Rowan-Robinson M., 1996, MNRAS, 283, 174
Rowan-Robinson M., Benn C. R., Lawrence A., McMahon R. G., Broadhurst T. J., 1993, MNRAS, 263, 123
Rowan-Robinson M., Saunders W., Lawrence A., Leech K., 1991, MNRAS, 253, 485
Rowan-Robinson M. et al., 1998, in Cox P., Kessler M. F., eds, The Universe as seen by ***ISO***, ESA SP-427. ESA, Paris
Rush B., Malkan M. A., Spinoglio L., 1993, ApJS, 89, 1
Serjeant S., 1999, MNRAS, submitted
Serjeant S. et al., 1997, MNRAS, 289, 457
Serjeant S., Gruppioni C., Oliver S., 1998, MNRAS, submitted (astro-ph/9808259)
Siebenmorgen R., Starck J.-L., Sauvage M., Cesarsky D. A., Blommaert J., Ott S., 1998, ISOCAM Data Users Manual, Version 4.0 (SAI/95-222/Dc)
Starck J.-L., Aussel H., Elbaz D. et al., 1998, in Mamon G. A., Thuan T. X., Tran Thanh Van J., eds, Extragalactic Astronomy in the Infrared, Moriond Series in Astrophysics. Editions Frontieres, Gif-sur-Yvette, p. 509
Sutherland W., Saunders W., 1992, MNRAS, 259, 413
Xu C. et al., 1998, ApJ, 508, 576

This paper has been typeset from a TEX/LATEX file prepared by the author.